PNAS RESEARCH ARTICLE | APPLIED PHYSICAL SCIENCES

Programming hydrogel adhesion with engineered polymer network topology

Zhen Yang[a], Guangyu Bao[a,1], Ran Huo[a,1], Shuaibing Jiang[a], Xingwei Yang[b], Xiang Ni[a], Luc Mongeau[a,c], Rong Long[b], and Jianyu Li[a,c,2]

Edited by Zhigang Suo, Harvard University, Cambridge, MA; received May 9, 2023; accepted August 21, 2023

Hydrogel adhesion that can be easily modulated in magnitude, space, and time is desirable in many emerging applications ranging from tissue engineering and soft robotics to wearable devices. In synthetic materials, these complex adhesion behaviors are often achieved individually with mechanisms and apparatus that are difficult to integrate. Here, we report a universal strategy to embody multifaceted adhesion programmability in synthetic hydrogels. By designing the surface network topology of a hydrogel, supramolecular linkages that result in contrasting adhesion behaviors are formed on the hydrogel interface. The incorporation of different topological linkages leads to dynamically tunable adhesion with high-resolution spatial programmability without alteration of bulk mechanics and chemistry. Further, the association of linkages enables stable and tunable adhesion kinetics that can be tailored to suit different applications. We rationalize the physics of polymer chain slippage, rupture, and diffusion at play in the emergence of the programmable behaviors. With the understanding, we design and fabricate various soft devices such as smart wound patches, fluidic channels, drug-eluting devices, and reconfigurable soft robotics. Our study presents a simple and robust platform in which adhesion controllability in multiple aspects can be easily integrated into a single design of a hydrogel network.

polymer gels | hydrogel adhesives | controlled adhesion | polymer entanglement

Significance

Programming hydrogel adhesion in multiple aspects including adhesion energy, kinetics, and spatial distribution can enable and improve various applications in engineering and medicine yet remains challenging in synthetic hydrogel adhesives. Existing paradigms rely on the addition of chemistries, function materials, or external apparatus, so that the complexity and incompatibility among different components complicate the adhesion programming. Here, we present that engineering the surface network topology of a hydrogel adhesive enables embodied programmable adhesion, including controllable adhesion energy, kinetics, and spatial distribution. This robust and versatile strategy works for highly uncontrolled targeted substrates such as biological tissues and enables the design of numerous soft devices such as a selective wound patch.

The precise programming of hydrogel adhesion, including its magnitude, kinetics, and spatial distribution, has significant implications for engineering, biology, and medicine. The ability to control adhesion energy is essential for bonding reinforcement or easy detachment after placement (1–3), while the ability to control adhesion spatially is useful for applications requiring varying adhesion properties on the targeted surface such as wound dressings (4). While most current research has focused on the adhesion magnitude at the equilibrium stage, controlling adhesion kinetics, which involves modulating transient adhesion over time, is less explored but equally important as it allows for tuning the operating time window for adhesive placement. As such, programming the multifaceted nature of hydrogel adhesion could enable and improve various applications ranging from tissue repair to soft robotics. However, such programmable adhesion is difficult to achieve for synthetic adhesives because they require the addition of complex chemistry and apparatus that are potentially difficult to integrate. For instance, tough hydrogels with covalent bond-based adhesion provide robust adhesion to diverse surfaces (5), but it is challenging to modulate their adhesion without introducing specific chemistry (6). In contrast, physical interactions offer more flexibility to modulate hydrogel adhesion energy, but they require specific material properties (e.g., viscoelasticity) or additional apparatus (light, ultrasound, etc.) (7–9). In terms of controlling adhesion kinetics, the rate of covalent bonding is fundamentally limited by the specific chemical reactions involved. Physical interactions such as the hydrogen bond often form instantaneously (10), providing limited tunability in terms of adhesion kinetics. Achieving spatial control of adhesion requires sophisticated patterning and treatment of the opposing surface (11, 12), and the outcome could be compromised by uncontrolled diffusion of chemical reagents, especially when the two adherends are sufficiently permeable (7). Selective masking of the opposing surface could enable spatially controlled adhesion (13–15), but may be difficult to perform on highly uncontrolled and unpredictable surfaces such as biological tissues. A universal design strategy that inherently allows for robust and multifaceted adhesion programming on diverse surfaces is still missing.

It has been found that cells utilize dynamic bonding through noncovalent protein–protein interactions, known as slip bonds (16, 17). These bonds exhibit dynamic adhesion strength, with a shorter lifetime under applied force due to the reduced energy barrier to bond rupture, allowing them to switch between bonding and motile states under different

Author contributions: Z.Y. and J.L. designed research; Z.Y., G.B., R.H., S.J., X.Y., and X.N. performed research; Z.Y. and R.L. contributed new reagents/analytic tools; Z.Y., G.B., X.Y., R.L., and J.L. analyzed data; and Z.Y., G.B., R.H., S.J., X.Y., L.M., R.L., and J.L. wrote the paper.

The authors declare no competing interest.

This article is a PNAS Direct Submission.

[1]G.B. and R.H. contributed equally to this work.

[2]To whom correspondence may be addressed. Email: jianyu.li@mcgill.ca.

This article contains supporting information online at https://www.pnas.org/lookup/suppl/doi:10.1073/pnas.2307816120/-/DCSupplemental.

Published September 19, 2023.

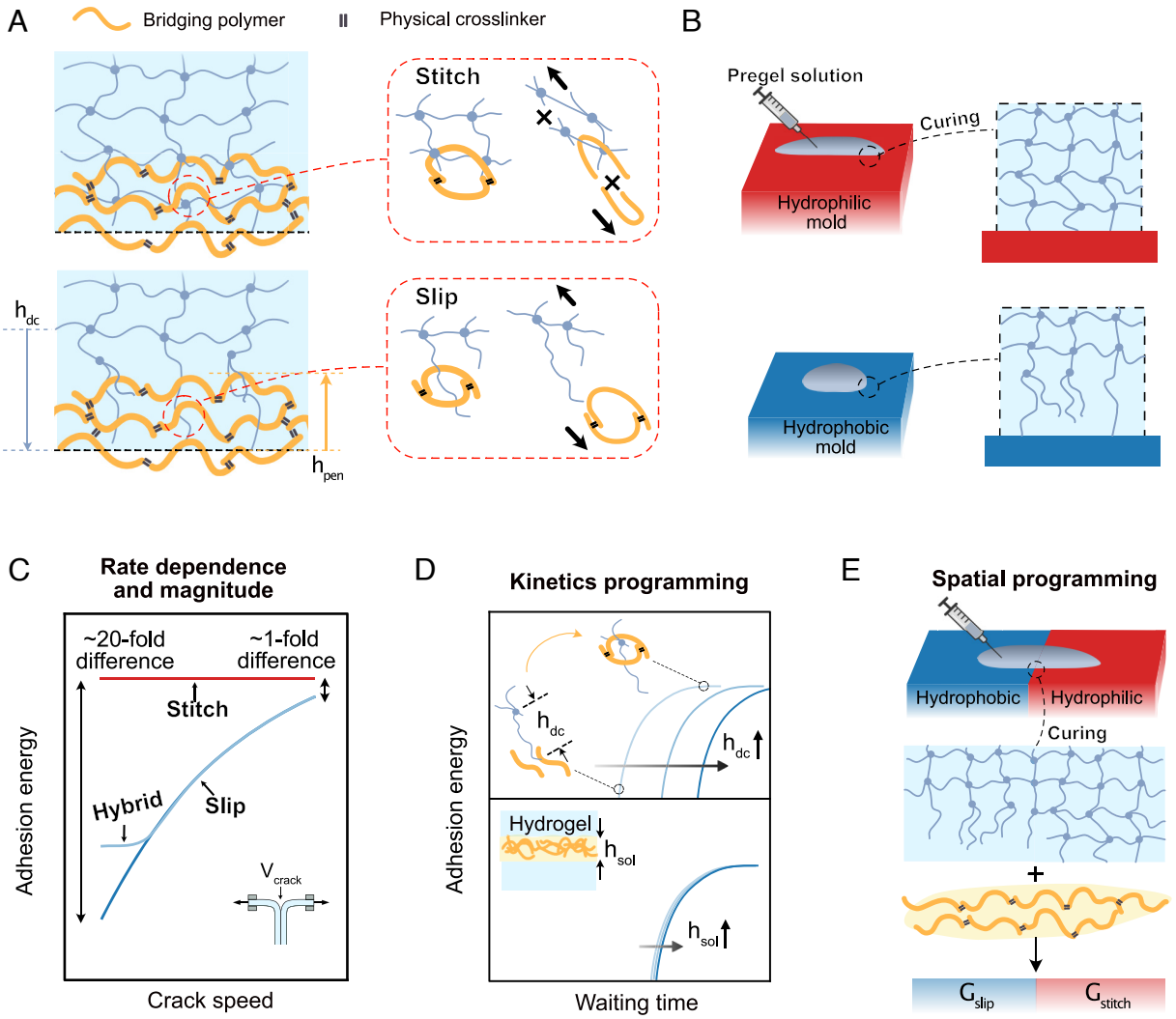

Fig. 1. Engineered network topology and linkages for multifaceted programming of hydrogel adhesion. (*A*) Schematics of the stitch linkage (*Top*) and slip linkage (*Bottom*) formed between a bridging polymer and networks without and with surface dangling chains. The thickness of the dangling chain layer and the penetration depth of the bridging polymer are denoted as h_{dc} and h_{pen}, respectively. (*B*) Hydrophilic and hydrophobic molds are used to form a regular network (*Top*) and a network carrying surface dangling chains (*Bottom*), respectively. (*C*) Rate dependence and magnitude of the adhesion energy depend on the interfacial linkage types: stitch linkages with $h_{pen}/h_{dc} \to \infty$, slip linkages with $h_{pen}/h_{dc} \ll 1$, and their hybrid with $h_{pen}/h_{dc} \approx 1$. (*D*) The slip linkage offers programmable adhesion kinetics through tuning h_{dc} (*Top*), which is also insensitive to processing conditions such as the thickness of bridging polymer solution h_{sol} (*Bottom*). (*E*) Spatially controllable adhesion obtained from patterning the topological linkages at the interface.

physiological environments (18). Furthermore, cells can achieve complex spatiotemporal adhesion controls (19, 20), which are not yet seen among synthetic hydrogel adhesives. In this study, we present an approach to engineer surface network topology in hydrogels, which enables the creation of polymer entanglement referred to as the slip linkage (Fig. 1*A*). The slip linkage has a topology of a long polymer chain entangled with another cross-linked network (chain-to-network) and can dissociate via chain slippage, a thermally activated process that results in dynamic adhesion analogous to slip bonds in cell adhesion. Both rate-dependence and magnitude of adhesion can be programmed through linkage design, enabling modulatable adhesion without background dissipation (Fig. 1*C*). Moreover, the kinetics of slip linkage association dominates over other subkinetics that are dependent on operating conditions. By carefully tuning the governing length scale, it is possible to control the kinetics of slip linkage association, resulting in a stable adhesion kinetics with adjustable half-time ranging from ~50s to ~1,000s (Fig. 1*D*). Furthermore, we demonstrate a simple fabrication method to pattern the slip linkage with another type of polymer entanglement, the stitch linkage, at the same interface (Fig. 1 *B* and *E*). The stitch linkage has the topology of two cross-linked polymer networks entangled together (network-to-network), as found in the hydrogel topological adhesion, and offers less tunability in terms of adhesion energy and kinetics (7). These two entanglement types display contrasting adhesion behaviors. When assembled on the interface, they allow for predefinable and spatially varying adhesion on diverse surfaces. Thus, our study provides an approach to embody multifaceted adhesion programmability into a hydrogel adhesive through a single design of the network structure. We refer to this approach as the topologically engineered adhesives (TEA), which offers a robust, facile, and predictive strategy for excellent control over hydrogel adhesion, and opens up numerous opportunities in engineering and medicine.

Results and Discussion

To robustly program hydrogel adhesion, we create a diffusive interface by placing a third species of diffusive polymer, called

bridging polymer, to the interface between hydrogel adhesives and targeted surfaces (7, 21). Formation of the chain-to-network topology of the slip linkage demands the following conditions: 1) The hydrogel network needs to contain dangling chains and 2) a thermodynamic driving force is needed to facilitate the diffusion of bridging polymers into the gel network. Meanwhile, the diffusion needs to be halted once the linkage forms to prevent the overdiffusion of bridging polymers into the bulk gel, which may reduce the number of linkages at the interface.

To meet the first condition, we choose polyacrylamide (PAAm) as a model hydrogel network and polymerize it on a mold with low surface tension such as Poly(methyl methacrylate) (PMMA). The hydrophobicity and other associated effects inhibit the free-radical polymerization of the gel in the vicinity of the mold (22–24).This effect results in a surface layer of branched dangling chains with thickness h_{dc} ranging from ∼10 to ∼100 μm estimated using our experimental results (described later), "protruding" from the cross-linked bulk network. This estimation is in reasonable agreement with an early study (23) showing that a layer of much lower polymer content forms near the surface of Teflon mold during the polymerization of poly-2-acrylamide2-methyl-1-propanesulfonic acid (PAMSP) and poly-acrylic acid (PAAc). The low polymer content layer has a thickness spanning over ∼100 μm, which manifests as a dangling chain layer when the gel fully cures. In contrast, gels polymerized on molds with high surface tension such as glass are not subject to the hydrophobic mold effect and hence contain cross-linked networks instead of branched dangling chains on their surfaces. The gels with and without engineered surface dangling chains are hereafter referred to as the TEA and regular gels, respectively. To meet the second criterion, stimuli-responsive polymers such as chitosan or gelatin were chosen as bridging polymers. The polarity between the hydrogel network and chitosan chains and the entropy of mixing together promote the diffusion of chitosan chains into the hydrogel; meanwhile, the chitosan chains can be triggered to cross-link into a bridging network through a reaction–diffusion process in responding to pH changes, leading to penetration depths h_{pen} on the order of tens of microns (21). Other strategies to form the chain-to-network topology of slip linkage at soft material interfaces are discussed in *SI Appendix*, Note 1.

Structural Characterization. Based on the above principles, we fabricate a model TEA using single-network TEA gel made of PAAm and select chitosan as the bridging polymer. To probe the engagement length between the dangling chains and the bridging polymer chains, we use confocal microscopy to visualize how fluorescently labeled chitosan chains penetrate the TEA gel at equilibrium. The fluorescence intensities exponentially decrease from the outermost surface to the bulk of the TEA gels with different cross-linker-to-monomer ratios C (colored dash lines, Fig. 2*A*). For different C, we measure similar distances where the intensities meet the lower plateau (black dash line, Fig. 2*A*), defining the penetration depth of the bridging polymer h_{pen} ≈70 μm. Note that h_{pen} may depend on the polydispersity of chitosan polymers (*SI Appendix*, Fig. S9). A systematic study with carefully controlled chitosan molecular weight and C varied in a wide range is needed for a holistic understanding of the relation between the h_{pen} and C. Further, this value may also depend on the reaction–diffusion process and thus may vary with the type of bridging polymers. For instance, h_{pen} for gelatin is expected to be temperature-dependent.

To confirm the presence of the dangling chain layer in TEA gels, we utilize scanning electron microscopy (SEM) to examine

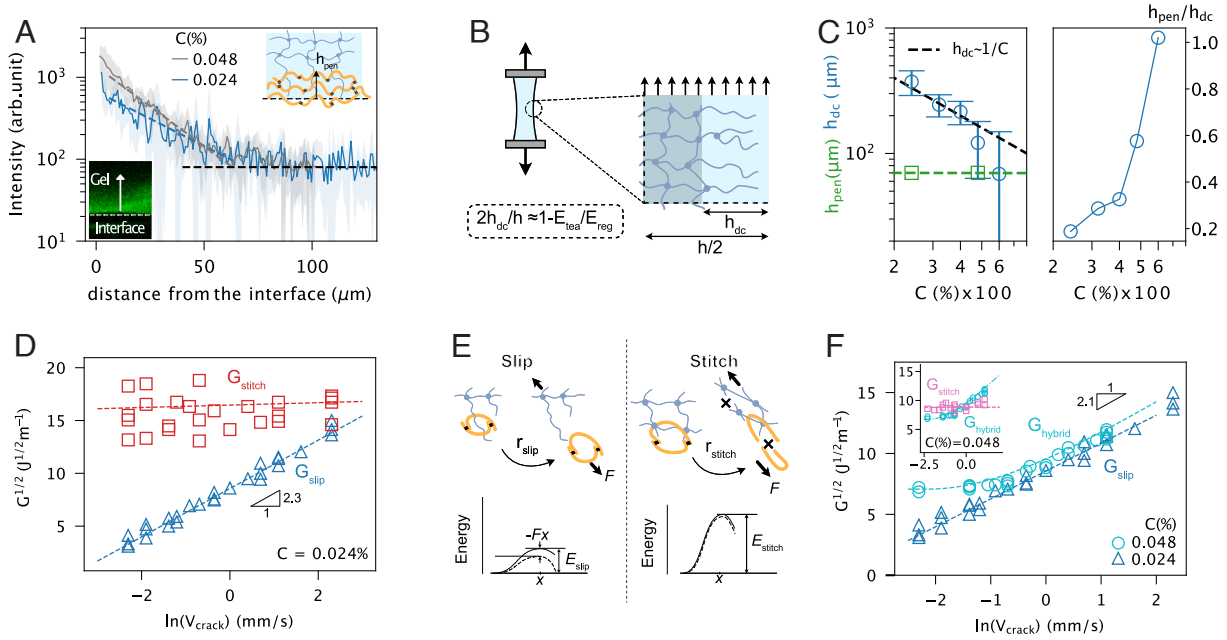

Fig. 2. Design and characterization of TEA. (*A*) Intensities of fluorescent chitosan chains diffused in TEA gels. The shaded area represents the SD from 5 measures. The stronger chitosan intensity for higher C may be due to more chitosan chains trapped by the denser dangling chains on the interface. (*B*) An idealized model used to estimate the thickness of the branched dangling chain layer. (*C*) *Left*: estimated h_{dc} and measured h_{pen} as functions of the cross-linker-to-monomer ratio C. Error bars represent SD. *Right*: relative engagement length h_{pen}/h_{dc} as a function of C. Dissimilar topological linkages lead to contrasting adhesion behaviors. (*D*) Slip and stitch linkages–mediated $G^{1/2}$ plotted as functions of ln(V_{crack}) for $C = 0.024\%$ and $c_{chi} = 2\%$ g/mL. (*E*) Illustration showing the dissociations of slip and stitch linkages as thermally activated processes, with the reaction rate of dissociation r_i (i can be slip or stitch). Upon a separation force F, the activation energy of the linkage is decreased by $-Fx$, where x is the separation distance. (*F*) The formation of topological linkages and the resulting adhesion depend on h_{pen}/h_{dc}, which is controlled by C. Slip and hybrid linkages are achieved for TEA gels with $C = 0.024\%$ and 0.048%, respectively. The inset shows the same curves as (*D*) but for $C = 0.048\%$.

a cryosectioned and dehydrated TEA gel sheet (100 μm thick, *SI Appendix*, Note 1 and Fig. S3). The dehydrated TEA gel sheet exhibits more pronounced edge shrinkage compared to a regular gel sheet. This phenomenon is presumably due to the lower polymer content and cross-linking density near the edge than in the bulk, indicating the presence of the dangling chain layer near the surface of TEA gels. Since directly imaging the dangling chains is challenging, we make a first-order estimation of the thickness h_{dc} of the dangling chain layer from the experimentally measured elastic moduli. The TEA gel has a total thickness of h and is idealized with a trilayer model (Fig. 2*B*): A layer of a regular network is sandwiched by two layers of branched dangling chains. The elastic modulus of the sandwiched regular network E_{reg} can be measured from a regular hydrogel formed at the same conditions except using a hydrophilic mold, given their observed structural similarity (23–25). The elastic modulus of the dangling chain layer is assumed to be negligible since it cannot carry any transverse loads when the applied tension is parallel to the gel surface. As such, we can estimate h_{dc} from the ratio of measured elastic moduli of the TEA and regular gels E_{tea}/E_{reg} in uniaxial tensile tests (Fig. 2*C* and *SI Appendix*, Note 1 and Fig. S1). We further perform microindentation test to ascertain the dangling chain layer thickness, and the results show reasonable agreement with the h_{dc} estimation from the uniaxial tensile test if considering the nonzero compressible modulus of the branched dangling chains (*SI Appendix*, Note 1). The estimations of h_{dc} show a decreasing trend with the increasing value of C. The trend $h_{dc} \sim C^{-1}$ may be attributed to the competition between bulk elasticity of the gel network and interface tension during gelation on hydrophobic mold (22) (*SI Appendix*, Note 1), demonstrating a controlled method for fabricating the dangling chain layer of different sizes.

With the measured length scales, we calculate their ratio h_{pen}/h_{dc} to quantify the extent to which the bridging polymers engage the dangling chains, which is expected to govern the formation of different topological linkages at the TEA gel interface (*SI Appendix*, Fig. S4*A*). When $h_{pen}/h_{dc} \ll 1$, the bridging network only engages a part of the dangling chain layer, so that the interface only comprises slip linkage. If $h_{pen}/h_{dc} \approx 1$, a complete engagement ensues which indicates that part of the bridging polymers may diffuse across the dangling chain layer to stitch the underlying network of the TEA gel. In this case, the linkage is expected to behave as the combination of the slip and stitch linkage and is referred to as the hybrid linkage (Fig. 1*C*). Last, a regular hydrogel interface that only comprises stitch linkage corresponds to $h_{pen}/h_{dc} \to \infty$ since $h_{dc} \to 0$. Fig. 2*C* shows $h_{pen}/h_{dc} \approx 0.2$ when $C = 0.024\%$ and increases to unity as C increases to 0.06% for the TEA gel interface. By tuning C, we can vary the degree of engagement and consequently the formation of different linkages, which will be shown later to modulate the resulting adhesion energy.

Interfacial Topological Linkages to Program Rate-Dependent Adhesion Energy. To test our hypothesis that topological linkages can be used to program adhesion, we first focus on two extremities: the interfaces containing either slip or stitch linkages. To form slip linkage-mediated adhesion, we adhere two TEA gels using chitosan as the bridging polymer with $h_{pen}/h_{dc} \approx 0.2$ ($C = 0.024\%$), followed by a T-peeling specimen to measure the adhesion energy G as a function of crack speed V_{crack} (*Methods*). Fig. 2*D* shows that the square root of the slip linkage-mediated adhesion $G^{1/2}$ varies logarithmically with V_{crack}, repetitively defined. We observe a factor of 25 in the change of G as V_{crack} varies by two decades. Together plotted in Fig. 2*D* is the stitch linkage-mediated adhesion formed between two regular hydrogels for the same C and chitosan concentration c_{chi}, showing higher magnitude but much weaker rate-dependence. The contrast between slip and stitch adhesion is the most pronounced at low V_{crack} but diminishes at high V_{crack}. We also observed adhesive failure and mixed adhesive-cohesive failure at the slip and stitch linkage–mediated interfaces, respectively. Our experiments further confirmed the similar bulk mechanics between the TEA and the regular gels: They both show minimal hysteresis in cyclic loadings and weak rate dependences, indicating near-perfect elasticity (*SI Appendix*, Fig. S1 *A–D*). The data suggest that different interfacial network topologies regulate hydrogel adhesion independent of the bulk properties.

These results motivate us to further analyze the data with a kinetic model proposed by Chaudhary (26). The model considers the breaking of linkages as thermally activated processes (26–29), and treats each linkage as a linear spring with stiffness k_i and an activation energy of dissociation E_i (i can be slip or stitch). These parameters influence the dissociation rates of the linkages (Fig. 2*E*), and consequently the rate-dependence of the hydrogel adhesion energy. As detailed in *SI Appendix*, Note 2, the model states the adhesion energy for linkage i relates to the crack speed via $G^{1/2} \sim \ln V_{crack}$, with the rate dependency and magnitude of the adhesion energy dictated by the slope and the intercept of the linear relation, respectively. Further, the model shows that the slope of the linear relation scales inversely to $k_i^{1/2}$ and the intercept depends on E_i while elevating c_{chi} simultaneously increases both the slope and the intercept. The model shows excellent agreement with our experimental data for different linkage types and varying c_{chi} (dash lines in Fig. 2*D* and *SI Appendix*, Fig. S5 *B* and *C*). By fitting this model to our data, we can determine k_i and E_i, which are otherwise difficult to characterize directly. Specifically, we find $k_{slip} = 1.7 \times 10^{-7}$ N/m and $E_{slip} = 75$ kJ/mol for the slip linkage with $C = 0.024\%$ and $h_{pen}/h_{dc} \approx 0.2$ (blue dash line, Fig. 2*D*). It is plausible that the hydrogel dangling chains that determine k_{slip} is of entropic type, which leads to $k_{slip} = 3k_BT/R^2$ with k_BT the energy in temperature and R the average end-to-end distance of the dangling chains. The model allows us to estimate $R \approx 250$ nm with the fitted value of k_{slip}, which is 50 times larger than the mesh size of the underlying network $\xi \approx 5$ nm (*SI Appendix*, Note 1). The fitted value of E_{slip} is larger than the typical activation energy of hydrogen bond (4–50 kJ/mol), suggesting potential synergistic contributions of multiple hydrogen bonds (between chitosan and PAAm) to a single slip linkage. Besides, the model captures the rate-insensitivity of $G_{stitch}^{1/2}$ of the stitch linkage with $k_{stitch} \gtrapprox 300k_{slip}$ and $E_{stitch} \approx 185$ kJ/mol (red dash line, Fig. 2*D*). The much larger k_{stitch} may be due to the full extension of the entangled networks prior to network rupture, driving the polymer chains far beyond the entropic limit. The estimation of E_{stitch} is in the range of the bond energy of the C–C bond (350 kJ/mol) (30) and the theoretically estimated energy stored in each bond prior to rupture using molecular parameters (60 kJ/mol) (31), in line with the assumption that the stitched networks must rupture during separation. This model reveals quantitatively that the slip linkages exhibit much lower stiffness and dissociation energy compared to those of stitch linkages, leading to their contrasting adhesion behaviors. This knowledge allows us to program adhesion energy, including rate dependency and magnitude, through linkage design.

Additionally, the model predicts that the hybrid linkage formed when h_{pen}/h_{dc} is close to 1, would impart tunable dependence on loading rate through the relation $G_{hybrid} = G_{slip} + G_{stitch}$. In this case, $G_{hybrid}^{1/2}$ is predicted to be a nonlinear function of ln V_{crack} with a finite and constant value of G_{stitch} (Fig. 1*C*), indicating that the hybrid linkage behaves as slip or stitch linkage, respectively, in different ranges of loading rates. To test the hypothesis, we prepared TEA gels with $h_{pen}/h_{dc} \approx 0.6$ ($C = 0.048\%$, Fig. 2*C*), and the resulting $G^{1/2}$ shows a nonlinear trend as expected: At high crack speed, the data collapse onto a master curve with that having $h_{pen}/h_{dc} \approx 0.2$ ($C = 0.024\%$), following $G_{slip}^{1/2} \sim \ln V_{crack}$ (Fig. 2*F*). Note that in this regime, the slip linkage-mediated adhesion is higher than that mediated by stitch linkage for the same C between two regular gels (Fig. 2 *F*, *Inset*). Below V_{crack} = 0.5 mm/s, the data converges to a plateau corresponding to rate-independent adhesion energy of ~50 Jm^{-2}. This baseline adhesion is also close to the value of G_{stitch} for the same C (~60 Jm^{-2}, Fig. 2 *F*, *Inset*), confirming the coexistence of stitch- and slip-linkages on the interface. Fixing G_{stitch} = 50 Jm^{-2}, our model captures the experimentally measured $G_{hybrid}^{1/2}$ with fitting parameters $k_{slip} = 1 \times 10^{-7}$ N/m and $E_{slip} = 71$ kJ/mol (Fig. 2*F*, cyan dot line), closed to the values of the sample with $h_{pen}/h_{dc} \approx 0.2$ ($C = 0.024\%$). The ability to control the type of linkage by tuning the entanglement length between TEA gel and bridging polymers offers a high level of adhesion programmability: Not only can we predictably tune the adhesion energy by varying loading rates, but also program varying rate dependence in different ranges of loading rate. The finite adhesion energy at low loading rates provided by the hybrid linkage can effectively prevent the adhesive from failing at static load to ensure good durability.

Programming Adhesion Kinetics. In addition to the equilibrium state of adhesion, we next demonstrate that the association of the topological linkages regulates the transient adhesion, which can be exploited to encode adhesion kinetics (Fig. 1*D*). When the bridging polymer solution is placed between the hydrogel and a permeable substrate, they diffuse into the two networks while simultaneously cross-linking into a bridging network in response to a trigger. The reaction–diffusion process comprises two concurrent subprocesses: the gelation and the diffusion of the bridging polymer with their kinetic time t_{gel} and t_d, respectively. We assume that the overall adhesion kinetics is governed by the slower subkinetics: $t \equiv \max\{t_d, t_{gel}\}$.

When using chitosan as the bridging polymer, the gelation process is due to the decrease of pH, which is associated with the diffusion of gelling trigger (protons) away from the cast adhesive solution. The thickness of the solution h_{sol} sets the critical diffusion length, and thus its kinetics time follows $t_{gel} \sim h_{sol}^2/D_{eff,gel}$ (32) where $D_{eff,gel}$ is the effective diffusion coefficient of the gelling trigger. However, h_{sol} is sensitive to the applied compression or wettability of the interface, yielding the gelation kinetics uncertain in practice without carefully controlled h_{sol}.

In contrast, the diffusion process of bridging polymers depends on the value of h_{dc}, and hence the type of formed linkages. For a regular gel, $h_{dc} \to 0$, the interface is dominated by stitch linkages which only require the bridging polymer to diffuse by one mesh size of the gel network, thus taking negligible kinetic time $t_d \approx 0$ s (32). As such, one can expect the adhesion kinetics of the regular hydrogel interface to be limited by t_{gel}, which is difficult to control in practice due to the variable h_{sol}. We hypothesize that incorporation of slip or hybrid linkages can resolve the issue. In this case, the formation of the linkages requires the bridging polymers to diffuse through the dangling chains layer (Fig. 3*A*),

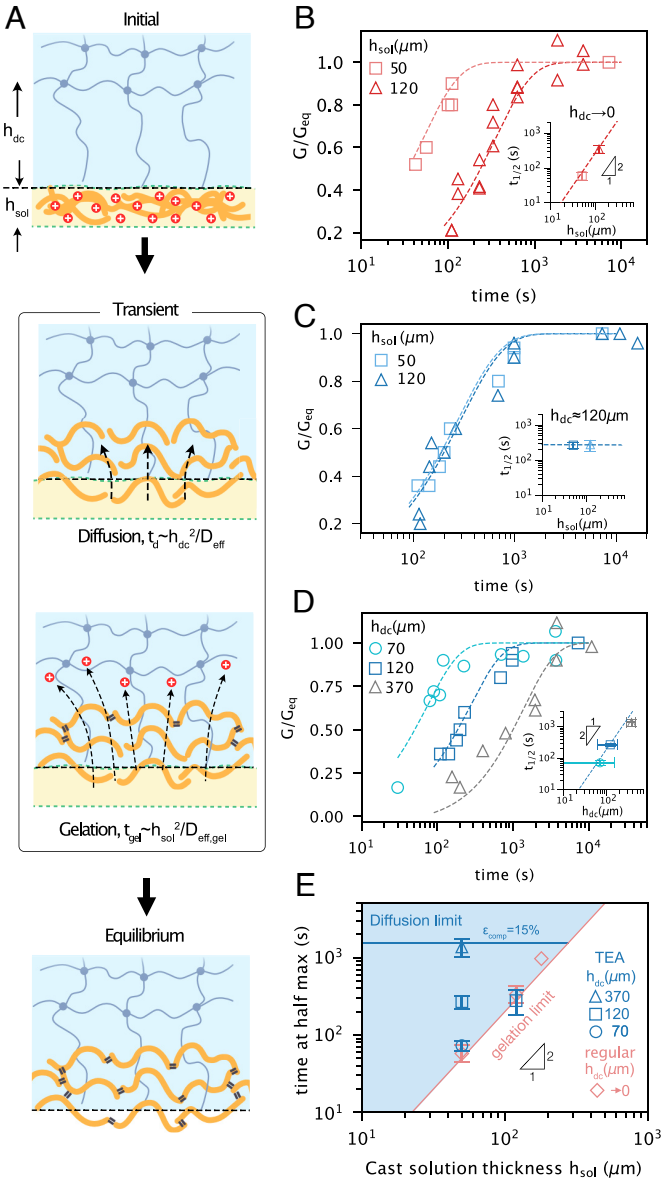

Fig. 3. Programmable adhesion kinetics of TEA. (*A*) Illustrations showing that the total adhesion kinetics comprises two subkinetic processes: diffusion and gelation. (*B*) Dimensionless adhesion between two regular hydrogels G/G_{eq} with G_{eq} = 49.98 Jm^{-2} and 47.42 Jm^{-2}, as functions of waiting time for cast solution thicknesses h_{sol} = 50 μm and 120 μm, respectively. The *Inset* shows $t_{1/2}$ as a function of h_{sol}. Error bars represent 95% CIs from fitting the exponential function. (*C*) Similar curves as (*B*) measured at the interface between two TEA gels with $h_{dc} \approx 120$ μm. G_{eq} = 48.10 Jm^{-2} and 47.4 Jm^{-2} for h_{sol} = 50 μm and 120 μm, respectively. (*D*) Adhesion kinetics of TEA interfaces with fixed h_{sol} (50 μm) and varying values of h_{dc} ($h_{dc} \approx 370, 120, 70$ μm, achieved using $C = 0.024\%$, 0.048%, and 0.06%, respectively). G_{eq} = 76.37 Jm^{-2}, 48.10 Jm^{-2} and 28.78 Jm^{-2}, for $h_{dc} \approx$ 370, 120, 70 μm, respectively. The *Inset* shows $t_{1/2}$ as a function of h_{dc}. The *y* error bars represent a 95% CI from fitting an exponential function while the x error bars represent the SD from 3 measures. (*E*) $t_{1/2}$ for regular ($h_{dc} \to 0$) and TEA gels (varying h_{dc}) plotted as functions of h_{sol}. The blue horizontal line corresponds to the TEA gel subject to an instantaneous compression of 15% strain without thickness-defining mesh (*SI Appendix*, Fig. S6*C*). The red diamond at h_{sol} = 180 μm is adapted from ref. 32.

so h_{dc} sets the characteristic diffusion length scale that yields $t_d \sim h_{dc}^2/D_{eff}$, where D_{eff} is the effective diffusion coefficient of the bridging polymers. The prolonged diffusion process can bypass the uncertain gelation process to govern the overall adhesion kinetics. Importantly, since h_{dc} is a material property, it can render the overall adhesion kinetics insensitive to processing or environmental conditions.

To test the hypothesis, we characterize the adhesion kinetics with different values of h_{sol} (50 and 120 μm) controlled by nylon meshes of different thicknesses (32) (*Materials and Methods* and *SI Appendix*, Fig. S6). We define the adhesion kinetics using the half-time $t_{1/2}$ when G reaches half of the equilibrium state value G_{eq}. For the regular gel interface, we observe a strong h_{sol}-dependent adhesion kinetics, and the associated kinetic time follows $t_{1/2} \sim h_{sol}^2$ (Fig. 3*B* and *Inset*). On the contrary, we notice that the adhesion kinetics of the TEA gel interface with $h_{dc} \approx 120$ μm ($C = 0.048\%$) is insensitive to the value of h_{sol} (Fig. 3*C* and *Inset*). Our point is further strengthened by applying an initial compression (15% strain) to the TEA gel interface ($h_{dc} \approx 370$ μm) without controlling h_{sol}, which yields the same adhesion kinetics as the TEA gel interface with controlled h_{sol} (*SI Appendix*, Fig. S6*C*). Thus, incorporation of the engineered dangling chain layer leads to adhesion kinetics insensitive to processing conditions, validating our hypothesis.

Importantly, not only is the TEA kinetics insensitive to processing conditions, but also it is controllable through changing h_{dc}. By fixing h_{sol}, we observe strong h_{dc}-dependent adhesion kinetics of the TEA gel interface: The kinetics accelerates as h_{dc} decreases, suggesting shorter distance that the bridging polymers need to diffuse across to form hybrid or slip linkages (Fig. 3*D*). The half-time follows $t_{1/2} \sim h_{dc}^2$ at $h_{dc} \approx 70$ and 120 μm. Fitting of the scaling relation to the data at these two h_{dc} values yields $D_{eff} \approx 5 \times 10^{-11} m^2 s^{-1}$ (*SI Appendix*, Table S4). This number roughly agrees with the value predicted by Rouse model (Fig. 3 *D*, *Inset* and *SI Appendix*, Note 3). Our data, however, deviate from the scaling relation at $h_{dc} \approx 370$ μm (Fig. 3 *D*, *Inset*). In the last case, the kinetics time is presumably bounded by the total diffusion-reaction time since $h_{pen}/h_{dc} \ll 1$, indicating that the underlying cross-linked network of the TEA gel is beyond the reach of bridging polymers.

Next, we discuss the role of each subkinetic process in determining the overall kinetics of TEA adhesion (Fig. 3*E*). In principle, the overall adhesion kinetics is a function of two key parameters: h_{dc} and h_{sol}, which govern the two subkinetics t_d and t_{gel}, respectively, i.e., $t_{1/2} \equiv \max\{t_d(h_{dc}), t_{gel}(h_{sol})\}$. A simple scaling analysis allows determination of the critical condition at which the limiting kinetic mechanisms switch: $h_{dc}^2 D_{eff,gel}/h_{sol}^2 D_{eff} = 1$. Taking $D_{eff,gel} \approx 10^{-11}$ m^2 s^{-1} (32) and $D_{eff} \approx 10^{-11}$ m^2 s^{-1} lead to $h_{dc} \approx h_{sol}$. When $h_{dc} \gg h_{sol}$ (the blue regime of Fig. 3*E*), $t_d \gg t_{gel}$, so that the $t_{1/2}$ of TEA gel is solely dependent on h_{dc} through $t_{1/2} \equiv t_d \sim h_{dc}^2/D_{eff}$. This allows us to tune the adhesion kinetics by varying h_{dc}. On the other hand, when $h_{dc} < h_{sol}$, the limiting kinetic mechanism switches due to $t_d < t_{gel}$, so that the adhesion kinetics is tunable by varying h_{sol} through $t_{1/2} \equiv t_{gel} \sim h_{sol}^2/D_{eff,gel}$. Therefore, the adhesion kinetics of the regular gels can be considered as a special case of TEA gels in the limit of $h_{dc} \to 0$, where the dominating kinetic mechanism is the gelation of the bridging polymers (indicated by the red line in Fig. 3*E*). The programmable TEA kinetics can be tailored to suit different applications. For instance, a small h_{dc} can be used with compression to achieve fast kinetics for hemostatic applications (33), while a large h_{dc} provides a sufficient and adjustable time window for adhesive placement.

We further note that h_{dc} in this study is reduced by increasing C, which tends to embrittle the bulk, and hence reducing the equilibrium adhesion energy G_{eq} of the TEA gel (Fig. 3*D*). For certain applications that demand both fast and strong adhesion, one could vary h_{dc} independently of C by polymerizing gels on molds with different hydrophobicity. This approach could enable the tuning of adhesion kinetics without changing G_{eq}. As a proof of concept, we demonstrate that a regular hydrogel, polymerized on a hydrophilic mold, contains negligible dangling chain layer $h_{dc} \to 0$ regardless of the value of C. Thus, a regular gel with relatively low cross-linking density $C = 0.024\%$ shows both fast adhesion kinetics (~70s with $h_{sol} = 50$ μm) and high G_{eq} (200 Jm^{-2}) due to the combination of small h_{dc} and small C (*SI Appendix*, Fig. S6*D*). This strategy enables the formation of fast and strong adhesion simultaneously.

Universal Applicability. The design and fabrication of TEA are universally applicable to a wide range of material systems, including various bridging polymers, targeted substrates, and TEA networks (Fig. 4*A*). We first examine a different bridging polymer gelatin in addition to chitosan. Gelatin is prepared as polymer solution at 37 °C and then applied to the interface between two TEA gels for $C = 0.024\%$ at room temperature. Similar to chitosan, gelatin diffuses into the gel and is cross-linked into a bridging network in responding to a temperature drop to form slip linkages with the TEA dangling chains. Our

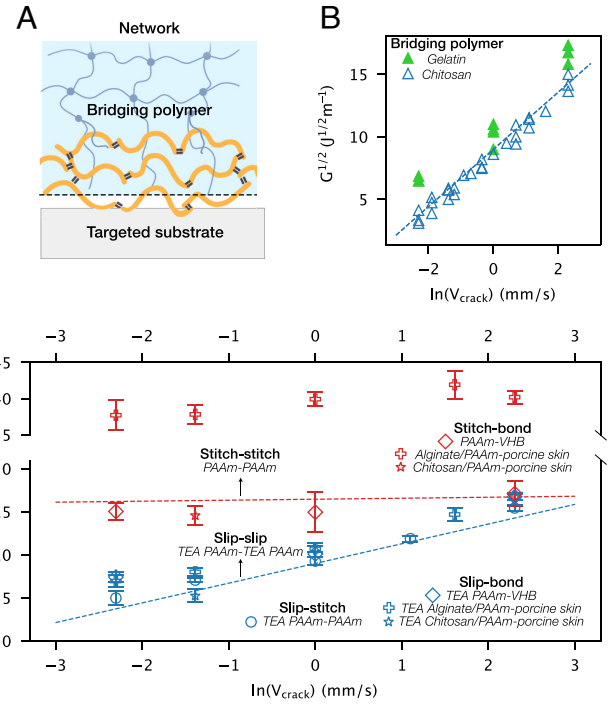

Fig. 4. Universal applicability of the TEA strategy. (*A*) Schematic showing that a TEA interface can be constituted by a variety of materials. (*B*) Slip–slip linage–mediated adhesion between two TEA gels using gelatin and chitosan as bridging polymers. $c_{chi} = c_{gelatin} = 2\%$ g/mL. (*C*) Topological linkages dictate hydrogel adhesion behaviors. The interfaces containing the slip linkage follow $G^{1/2} \sim \ln V_{crack}$, and the adhesion shows stronger rate-dependence compared to those not containing the slip linkage. The red and blue dash lines correspond to the stitch–stitch and slip–slip-mediated adhesion in Fig. 2*D*, respectively. The bridging polymer is chitosan with $c_{chi} = 2\%$ g/ml. The TEA gels have cross-linker density $C = 0.024\%$. The constituents of different topological linkages are listed in *SI Appendix*, Table S1.

data reveal an identical trend between the data obtained using gelatin and chitosan as bridging polymers (Fig. 4*B*), highlighting the dominating role of polymer topology rather than material chemistry in the formation of slip linkages.

Second, slip linkages formed at the gel-bridging network interface can be coupled with other interactions that the bridging network can interact with the targeted substrates, such as slip, stitch linkages, or covalent bonds (34). For instance, the triggered cross-linking and the abundant amino groups of chitosan chains provide numerous options to interact with diverse substrates through stitch linkage or covalent bonds (35). Based on the principle, slip–slip, slip–stitch, and slip–bond linkages were achieved between two TEA gels, between a TEA and a regular gel, and between a TEA gel and a VHB elastomer, respectively (*SI Appendix*, Table S1). Our data reasonably collapse for the three linkage types to engage different targeted substrates (Fig. 4*C*), suggesting that the overall adhesion behavior is dictated by the slip linkages while depending less on the types of interactions between the bridging network and targeted substrates. Without the slip linkage, the adhesion between two regular PAAm gels (stitch–stitch) and between a regular PAAm gel and a VHB elastomer (stitch–bond) shows much less rate-dependence and higher magnitude (Fig. 4*C*). These results validate the robustness of adhesion programming through the TEA strategy.

Last, we explore using double-network (DN) hydrogel as the TEA network, which exhibits much higher fracture toughness and adhesion (5, 21, 36, 37) due to background dissipation compared to single-network (SN) hydrogels. We test alginate/PAAm and chitosan/PAAm hydrogels as representative materials. In both types of DN gels, alginate and chitosan are physically cross-linked macromolecules and do not covalently interfere with the PAAm network, we expect that the hydrophobic mold could produce surface dangling chains in the PAAm network within the DN gels. We confirm the presence of the dangling chain layer in the surface of alginate/PAAm hydrogel polymerized on a hydrophobic substrate by EDTA treatment to remove calcium-alginate bonds followed by Atomic Force Microscopy (AFM) tests (*SI Appendix*, Fig. S7 *A* and *B*). We then examined the adhesion of TEA and regular DN gels that, respectively, polymerized on PMMA and glass molds to porcine skin (for a systematic study on different gelling molds, see *SI Appendix*, Fig. S7*C*). We use chitosan as the bridging polymer and EDC/NHS reagent to form covalent bonds between chitosan and tissue surfaces (21). Our data show that the adhesion of TEA alginate/PAAm gels on porcine skins (slip–bond) also follows $G^{1/2} \sim \ln V_{\text{crack}}$, with similar slope to those of SN TEA gels (slip–slip, slip–stitch, and slip–bond) (Fig. 4*C*). In contrast, the adhesion between regular alginate/PAAm gels and porcine skins (stitch–bond) show much higher adhesion energy with less rate-dependence within the tested range of crack speed. Further investigations are conducted with TEA chitosan/PAAm gels on porcine skins (slip–bond) at $V_{\text{crack}} = 0.25$ mm/s, also agreeing with those of SN TEA gels. In comparison, the adhesion between regular chitosan/PAAm gels and porcine skins (stitch–bond) is almost 10-fold higher (37) than the TEA counterpart, consistent with the adhesion of SN regular gels (Fig. 4*C*). The results demonstrate that our methodology is not only applicable to SN hydrogels but also DN hydrogels as long as the topology of one of the networks can be engineered.

Programming Spatial Adhesion. The contrast between slip and stitch linkages allows us to program the adhesion spatially. To do so, we pattern a mold substrate with hydrophilic (Glass) and hydrophobic regions (PTFE films thickness ~0.1 mm), followed by polymerizing a TEA gel on the patterned mold (*SI Appendix*, Fig. S7*D*). While the unequal thicknesses of the hydrophilic and hydrophobic regions can influence the flatness of the resulting gel, we perform a separate experiment with varying thickness mismatch between the hydrophilic and hydrophobic regions (±0.1 mm) to confirm that the flatness does not affect the adhesion selectivity (*SI Appendix*, Fig. S7*E*). Given the predefined geometries (circle, triangle) of the hydrophobic domains, we can design the dangling chain region where weak adhesion G_{slip} is formed at low loading rates; meanwhile, strong adhesion G_{stitch} is formed in other areas to sustain tension or twisting applied to the interface without interface debonding. Fig. 5*A* and *SI Appendix*, Fig. S7*F* show that by shaping the dangling chain region, we can achieve weak adhesion region of complex shapes between a TEA gel and a regular gel. To further characterize the resolution of the spatially programmable adhesion, we make a series of circular islands of nominal radii r_{nominal} in which slip linkages are formed. By slowly injecting the liquid dye, we visualize and measure their radii r_{measure} of the weak adhesion region using a digital camera (Fig. 5*B*). The excellent agreement between the nominal and measured radii suggests high spatial resolution ~0.1 mm is achieved with a manual procedure. Moreover, the one-step fabrication allows spatially heterogeneous adhesion to be assembled within a piece of monolithic hydrogel, which otherwise requires assembling different materials at the interface. This could be conducted beforehand and using 3D-shaped substrates for curved adhesive surface. It is beneficial when soft, wet, and curved biological tissues are involved, as the hydrogel interface is inherently soft and mechanically compatible with such tissues. There exist other strategies such as selective masking for creating spatial heterogeneity in adhesion (13–15). Selective masking is a facile approach, but its implementation may involve the placement of masking materials, often made of rigid polymer films, which could be complicated by the mechanical mismatch and unwanted adhesion on substrates such as biological tissues. Furthermore, substrate patterning procedures are time-consuming and may not suit time-sensitive scenarios such as surgical applications. In contrast, our method directly encodes the patterned adhesion into the soft and deformable hydrogel interface (38, 39), thereby alleviating the need for masking materials.

As the slip and stitch linkages show different sensitivities to loading rate, we expect the spatially selective adhesion, characterized by the adhesion energy contrast $G_{\text{slip}}/G_{\text{stitch}}$, to be also rate-dependent. Fig. 5*C* shows that $G_{\text{slip}}/G_{\text{stitch}}$ predicted by the parameterized model (*SI Appendix*, Note 2) approaches unity at high V_{crack} and decreases toward zero at low V_{crack}. The prediction is supported by our experimental observations: A TEA gel with the designed dangling chain region shows large adhesion contrast to a regular gel at low V_{crack}, while the interface appears to be uniformly adhesive at relatively larger V_{crack} (Fig. 5*D*). The rate-dependent and spatially programmable adhesion can potentially enable applications which desire tunable adhesion contrast in different regions under varying loading rates. Additionally, not only we can achieve reduced adhesion ($G_{\text{slip}}/G_{\text{stitch}} < 1$) but also enhanced adhesion ($G_{\text{hybrid}}/G_{\text{stitch}} > 1$) in the engineered dangling chain region at large V_{crack} (*SI Appendix*, Fig. S4*B*). In this case, the slip linkage acts as a toughener that synergistically contributes to the adhesion with the stitch linkage.

TEA-based Devices. The programmable adhesion of TEA enables various applications such as wound patches, drug depots, fluidic channels, and soft actuators. For the application of wound

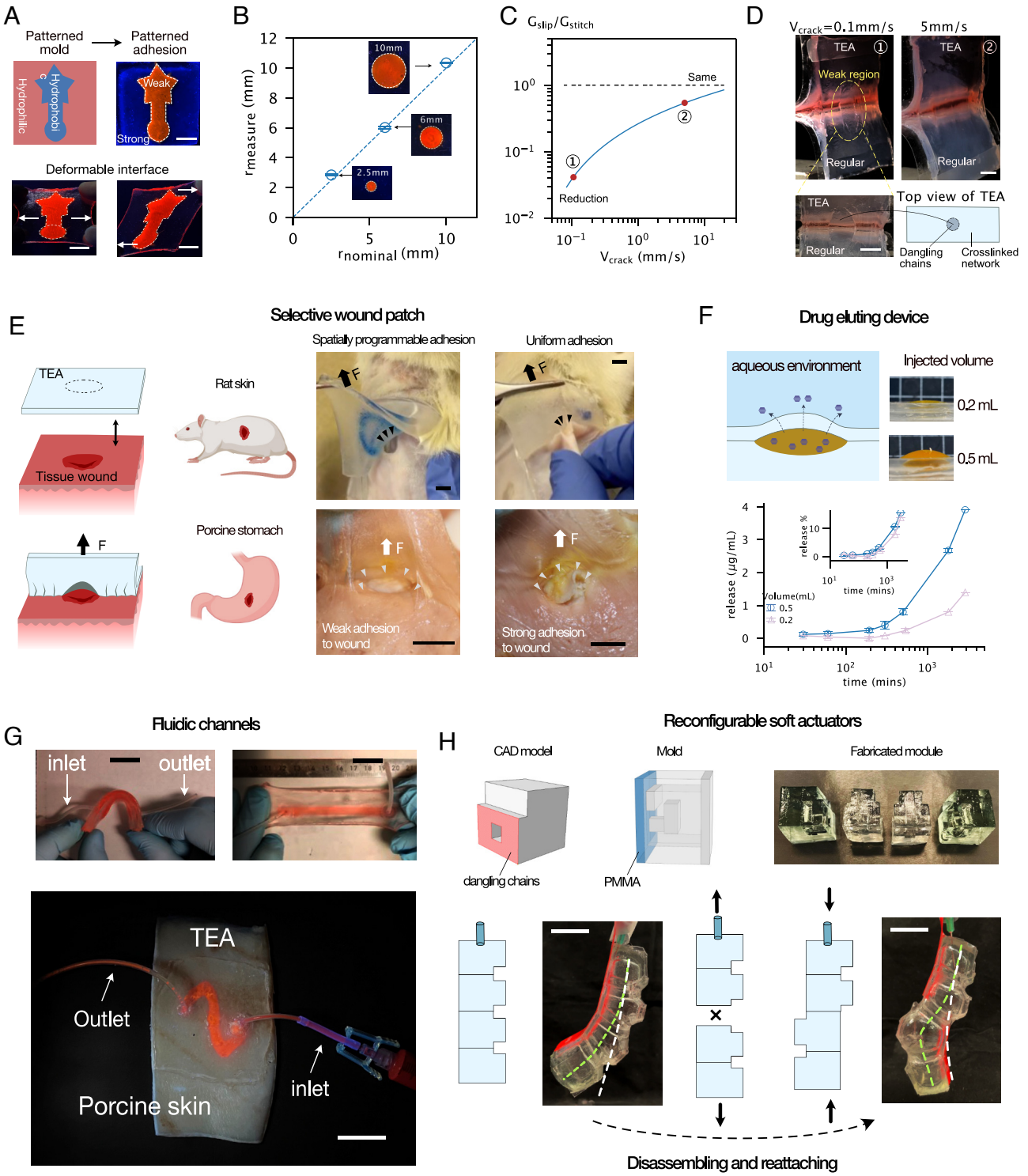

Fig. 5. Spatial programming and soft devices enabled with TEA. (*A*) TEA strategy enables spatially programmable and deformable adhesion between a TEA alginate/PAAm gel and a regular alginate/PAAm gel. The patterned adhesion is visualized by slow injection of liquid dye into the weak interface. (Scale bar: 1 cm.). (*B*) Spatial resolution of the spatially programmable adhesion. (*C*) Predicated adhesion energy contrast G_{slip}/G_{stitch} achieved using the parameterized model (*SI Appendix*, Eq. **S14**) using the data of G_{slip} and G_{stitch} in Fig. 2*D*. (*D*) Experimental demonstration of the rate-dependent G_{slip}/G_{stitch} between a SN TEA gel with a circular-shaped dangling chain region and a SN regular gel (Scale bar: 1 cm.). (*E*) Wound patches made of TEA and regular alginate/PAAm gels adhered to wounds on rat skin (*Top*, Scale bar: 8 mm.) and porcine stomach (*Bottom*, Scale bar: 12 mm.). (*F*) A drug-eluding device enabled by injecting drug into the weakly adhered interface between a SN TEA gel and a SN regular gel. Grid size of the *Inset*: 10 mm. (*G*) Deformable hydrogel-based fluidic channels created by adhering a TEA alginate/PAAm gel to a regular alginate/PAAm gel (Scale bar: 2 cm.). (*Bottom*) A TEA alginate/PAAm gel with designed adhesion selectivity forms a fluid channel on the surface of a porcine skin (Scale bar: 2.5 cm.). (*H*) Reconfigurable soft actuators. (*Top*) The fabrication process of the actuator units with connection surfaces composed of dangling chains. (*Bottom*) Two modes of actuation. The initial and the actuated stages are indicated by the white and green dash lines, respectively (Scale bars: 2 cm.).

patches, TEA allows for programming weak adhesion to wound beds while maintaining strong adhesion to the surrounding healthy tissue. As such, the patch could protect the wound without impairing tissue regeneration and wound closure. Using the one-step fabrication process (Fig. 1*E* and *SI Appendix*, Fig. S7*D*), we prepare such a TEA gel with its surface composed of a circular region of dangling chains and the surrounding region of cross-linked network. The dangling chain region forms slip linkages which attach weakly to the wound site upon slow removal to minimize the damage to the wound. Meanwhile, the stitch linkages attach strongly to the surrounding healthy tissue to maintain the stickiness of the patch. In contrast, a regular hydrogel exerts strong and uniform adhesion to both wounded and healthy tissues, which ruptures the wound bed upon removal (Fig. 5*E*).

Besides, the creation of a weak adhesion region between two hydrogels could serve as a drug depot. Upon slow injection, mock drug solution fills up the weak interface. Further injection creates a bulge of hydrogel to accommodate a high amount of drug, which can be continuously released through the hydrogel network when the whole device is immersed in an aqueous environment (Fig. 5 *F*, *Top*). Our data show that the initial amount of drug injected into the depot affects the amount of release over time but the relative kinetics of release remains similar (Fig. 5 *F*, *Bottom*). As well, we can create a drug depot above a wound site, where drugs can be directly released into wounded tissue. In contrast, the strong adhesion of a regular hydrogel prevents the injection of drug solution to interface (*SI Appendix*, Fig. S7*G*).

We then demonstrate hydrogel-based fluidic devices assembled with TEA. A alginate/PAAm TEA DN gel with a rectangular-shaped dangling chain region forms a partially weak interface with a regular DN gel, which subsequently becomes a fluidic channel upon slow injection of liquids. The resulting device is highly deformable while no liquid leakage is observed (Fig. 5 *G*, *Top*). The one-step fabrication technique provides a simple approach to fabricate hydrogel fluidic channels compared with conventional methods that typically involve multiple molding steps (40, 41). In addition, the spatially programmable adhesion is applicable to varying surfaces as it requires no patterning of the targeted substrate. As such, we can form such a fluid channel directly on tissue surfaces such as porcine skin (Fig. 5 *G*, *Bottom*). This feature could benefit the design of medical devices that contact with tissue surfaces for sustained drug release (42), or in-vitro organ-on-chip models to study cellular behaviors (43).

Last, we show that the TEA made of SN PAAm hydrogels can be used to construct reconfigurable soft actuators, featuring minimal bulk dissipation for efficient actuation and dynamic adhesion for reversible attachment (Fig. 5*H*). Such actuators are formed with hydrogel units that contain surface dangling chains on each face and are connected to each other with the aid of bridging polymer (*Materials and Methods*). The slip linkage-mediated adhesion between the units is strong enough to sustain actuation yet can be separated easily and slowly with a small force. The separated units can then be reconnected upon reapplying the bridging polymer solution to the interface so that one can modify configurations of assembly for different actuation. Our data show that the slip linkage-mediated adhesion increases and reaches a plateau after cycles of detachment and reattachment (*SI Appendix*, Fig. S5*D*). This property can be partially attributed to the fact that the dissociation of the slip linkage only involves chain slippage, hence not rupturing the adherend networks (*SI Appendix*, Fig. S5*E*). Thus, the slip-mediated TEA interface is inherently subjected to minimal damage compared with those bonded by stitch linkages or covalent bonds.

Conclusion

In summary, we have demonstrated that designing the interfacial network topologies of hydrogels provides a facile and robust approach to program adhesion in multiple aspects including magnitude, space, and kinetics. Our approach can be potentially extended to different length scales using proper manufacturing processes. For instance, spatially programmable adhesion with a spatial resolution on the microscale can be achieved with microfabrication of the hydrogel network topology (44, 45), while that on the meter scale is expected to be achieved using gelling molds of the same size for applications such as camouflaging skin (46). Broadly, our methodology falls into the emerging paradigm of material intelligence, as the adhesion programming is directly encoded in the hydrogel network as material properties, similar to other properties such as elastic modulus. The implementation of adhesion control requires no external apparatus, making the methodology extremely facile, robust, and scalable. We hope that the design of TEA can spark interest in controlling hydrogel adhesion by designing their network topologies, opening the door to a broad design space for intelligent materials/structures through programmable adhesion.

Materials and Methods

Materials. All chemicals were purchased and used without further purification. Materials for the hydrogel synthesis and the bridging polymer include acrylamide (AAm, Sigma-Aldrich, A9099), N,N′-methylenebisacrylamide (MBAA; Sigma-Aldrich, M7279), ammonium persulfate (APS, Sigma-Aldrich, A3678), N,N,N′,N′-tetramethylethylenediamine (TEMED, Sigma-Aldrich, T7024), Alginate (I-1G) was purchased from KIMICA Corporation, chitosan (degree of deacetylation, DDA: 95%, medium- and high-molecular weight, Lyphar Biotech), sodium bicarbonate (Fisher Scientific, S233), sodium phosphate monobasic (NaH2PO4, Sigma, S8282), sodium phosphate dibasic (Na2HPO4, Sigma-Aldrich, S7907), acetic acid (Sigma-Aldrich, A6283), calcium sulfate (Sigma-Aldrich), N-hydroxysulfosuccinimide (NHS, Sigma-Aldrich, 130672), and 1-ethyl-3-(3-dimethylaminopropyl) carbodiimide (EDC, Sigma-Aldrich, 03450), Gelatin (Sigma-Aldrich, G2500). Glass, acrylic sheets (PMMA), PS, silicon, and PTFE were purchased from McMaster-Carr to make mold substrates for polymerization. VHB elastomer was purchased from 3M. Porcine skin was purchased from a local grocery store, then stored in a fridge at −20 °C, and thawed at 4 °C before use. Nylon mesh was purchased from McMaster Carr without further modification (9318T25, 9318T23 for thicknesses of 50 μm and 120 μm, respectively.).

Synthesis of TEA. The single network PAAm TEA gels were prepared as follows. AAm monomers of 6.76 g were first dissolved in 50 mL of deionized water. After degassing, the AAm solution of 25 mL was mixed with varying amounts of MBAA aqueous solution (0.02 g mL^{-1}) and 20 μL of TEMED in a syringe. The volumes of MBAA solution added were 90, 120, 150, 180, and 240 μL for the cross-linker—to—monomer molar ratios C at 0.024%, 0.032%, 0.04%, 0.048%, 0.06%, respectively. Meanwhile, another syringe was added with 565 μL of APS solution (0.066 g mL^{-1}) and 478 μL deionized water. The two syringes were connected with a Luer—Lock connector, so the two solutions were syringe—mixed to form a homogeneous solution. The mixture was immediately injected into rectangular acrylic molds of 80 × 20 × 3 mm^3 or 80 × 15 × 1.5 mm^3, covered with PMMA on both sides, and then kept at room temperature for 24 h to complete the reaction. To prepare the regular PAAm gels, we follow the same procedure except for injecting the mixed solution into the acrylic molds covered by glass sheets on the two sides. The synthesis of double network TEA gels is similar to that for the single network TEA gels and is detailed in *SI Appendix*.

Preparation of the Bridging Polymer Solutions. This study tested two types bridging polymers: chitosan and gelatin. To prepare the chitosan solutions of 2%, 1%, and 0.5% w/v, 50 mL of deionized water was added with chitosan powders of 1, 0.5, 0.25 g, respectively. 400 μL of acetic acid was also added for a final pH of 4.5. The mixture was stirred overnight to form a homogeneous solution and then kept at 4 °C before use. To prepare the gelatin solution of 2% w/v, 1 g of gelatin powder was dissolved in 50 mL of deionized water. The solution was stirred in a water bath at 37 °C for 30 min before use.

All details associated with sample preparations, mechanical tests, derivation and calibration of the thermally activated chain slippage model, and estimation of the diffusion coefficients of bridging polymers can be found in *SI Appendix*.

Data, Materials, and Software Availability. All study data are included in the article and/or *SI Appendix*.

ACKNOWLEDGMENTS. This work is supported by the Natural Sciences and Engineering Research Council of Canada (grant RGPIN-2018-04146), Fonds de Recherche du Quebec-Nature et technologies (grants FRQNT PR-281851), and the National Institute on Deafness and Other Communication Disorders (grant R01-DC018577). Z.Y. and R.H. acknowledge support from FRQNT and McGill Engineering Doctoral Award. S.J. acknowledges support from FRQNT Doctoral Award. X.Y. and R.L. acknowledge support from the NSF of the United States (NSF CMMI-1752449). J.L. acknowledges the support from the Canada Research Chair Program. We acknowledge Mr. Tianqin Ning and Mr. Yixun Chen for taking pictures, Mr. Omar Peza-Chavez for helping with cryosectioning.

Author affiliations: [a]Mechanical Engineering, McGill University, Montreal, QC H3A 0C3, Canada; [b]Mechanical Engineering, Colorado University Boulder, Boulder, CO 80309; and [c]Biomedical Engineering, McGill University, Montreal, QC H3A 2B4, Canada

1. Z. Yang, X. Yang, R. Long, J. Li, Stimulation modulates adhesion and mechanics of hydrogel adhesives. *Langmuir* **37**, 7097–7106 (2021).
2. H. Cho *et al*., Intrinsically reversible superglues via shape adaptation inspired by snail epiphragm. *Proc. Natl. Acad. Sci. U.S.A.* **116**, 13774–13779 (2019).
3. A. B. Croll, N. Hosseini, M. D. Bartlett, Switchable adhesives for multifunctional interfaces. *Adv. Mater. Technol.* **4**, 1900193 (2019).
4. S. Blacklow *et al*., Bioinspired mechanically active adhesive dressings to accelerate wound closure. *Sci. Adv.* **5**, eaaw3963 (2019).
5. H. Yuk, T. Zhang, S. Lin, G. A. Parada, X. Zhao, Tough bonding of hydrogels to diverse non-porous surfaces. *Nat. Mater.* **15**, 190–196 (2016).
6. X. Chen, H. Yuk, J. Wu, C. S. Nabzdyk, X. Zhao, Instant tough bioadhesive with triggerable benign detachment. *Proc. Natl. Acad. Sci. U.S.A.* **117**, 15497–15503 (2020).
7. J. Yang, R. Bai, Z. Suo, Topological adhesion of wet materials. *Adv. Mater.* **30**, 1800671 (2018).
8. Y. Gao, K. Wu, Z. Suo, Photodetachable adhesion. *Adv. Mater.* **31**, 1806948 (2019).
9. Z. Ma *et al*., Controlled tough bioadhesion mediated by ultrasound. *Science* **377**, 751–755 (2022).
10. Y. Wang *et al*., Instant, tough, noncovalent adhesion. *ACS Appl. Mater. Interfaces* **11**, 40749–40757 (2019).
11. E. P. Chan, D. Ahn, A. J. Crosby, Adhesion of patterned reactive interfaces. *J. Adhesion* **83**, 473–489 (2007).
12. J. M. Dugan, C. Colominas, A. A. Garcia-Granada, F. Claeyssens, Spatial control of neuronal adhesion on diamond-like carbon. *Front. Mater.* **8**, 756055 (2021).
13. H. Yuk, T. Zhang, G. A. Parada, X. Liu, X. Zhao, Skin-inspired hydrogel-elastomer hybrids with robust interfaces and functional microstructures. *Nat. Commun.* **7**, 12028 (2016).
14. W. Lee, J. Lim, J. Kim, Conformal hydrogel-skin coating on a microfluidic channel through microstamping transfer of the masking layer. *Anal. Chem.* **95**, 8332–8339 (2023).
15. D. C. Young, I. G. Newsome, J. Scrimgeour, Incorporation of soft shaped hydrogel sheets into microfluidic systems using a simple adhesion masking process. *Appl. Phys. Lett.* **111**, 263705 (2017).
16. S. Rakshit, Y. Zhang, K. Manibog, O. Shafraz, S. Sivasankar, Ideal, catch, and slip bonds in cadherin adhesion. *Proc. Natl. Acad. Sci. U.S.A.* **109**, 18815–18820 (2012).
17. V. Barsegov, D. Thirumalai, Dynamics of unbinding of cell adhesion molecules: Transition from catch to slip bonds. *Proc. Natl. Acad. Sci. U.S.A.* **102**, 1835–1839 (2005).
18. R. P. McEver, C. Zhu, Rolling cell adhesion. *Annu. Rev. Cell Dev. Biol.* **26**, 363–396 (2010).
19. P. W. Oakes, S. Banerjee, M. C. Marchetti, M. L. Gardel, Geometry regulates traction stresses in adherent cells. *Biophys. J.* **107**, 825–833 (2014).
20. M. E. Berginski, E. A. Vitriol, K. M. Hahn, S. M. Gomez, High-resolution quantification of focal adhesion spatiotemporal dynamics in living cells. *PLoS ONE* **6**, e22025 (2011).
21. J. Li *et al*., Tough adhesives for diverse wet surfaces. *Science* **357**, 378–381 (2017).
22. J. P. Gong, A. Kii, J. Xu, Y. Hattori, Y. Osada, A possible mechanism for the substrate effect on hydrogel formation. *J. Phys. Chem. B* **105**, 4572–4576 (2001).
23. A. Kii, J. Xu, J. P. Gong, Y. Osada, X. Zhang, Heterogeneous polymerization of hydrogels on hydrophobic substrate. *J. Phys. Chem. B* **105**, 4565–4571 (2001).
24. J. Mandal *et al*., Oxygen inhibition of free-radical polymerization is the dominant mechanism behind the "mold effect" on hydrogels. *Soft Matter* **17**, 6394–6403 (2021).
25. K. Zhang, R. Simic, W. Yan, N. D. Spencer, Creating an interface: Rendering a double-network hydrogel lubricious via spontaneous delamination. *ACS Appl. Mater. Interfaces* **11**, 25427–25435 (2019).
26. M. K. Chaudhury, Rate-dependent fracture at adhesive interface. *J. Phys. Chem. B* **103**, 6562–6566 (1999).
27. E. Evans, K. Ritchie, Dynamic strength of molecular adhesion bonds. *Biophys. J.* **72**, 1541–1555 (1997).
28. G. I. Bell, Models for the specific adhesion of cells to cells: A theoretical framework for adhesion mediated by reversible bonds between cell surface molecules. *Science* **200**, 618–627 (1978).
29. I. V. Pobelov *et al*., Dynamic breaking of a single gold bond. *Nat. Commun.* **8**, 15931 (2017).
30. C. Creton, M. Ciccotti, Fracture and adhesion of soft materials: A review. *Rep. Progr. Phys.* **79**, 046601 (2016).
31. S. Wang, S. Panyukov, M. Rubinstein, S. L. Craig, Quantitative adjustment to the molecular energy parameter in the Lake–Thomas theory of polymer fracture energy. *Macromolecules* **52**, 2772–2777 (2019).
32. J. Steck, J. Kim, J. Yang, S. Hassan, Z. Suo, Topological adhesion. I. Rapid and strong topohesives. *Extr. Mech. Lett.* **39**, 100803 (2020).
33. G. Bao *et al*., Liquid-infused microstructured bioadhesives halt non-compressible hemorrhage. *Nat. Commun.* **13**, 5035 (2022).
34. J. Yang, R. Bai, B. Chen, Z. Suo, Hydrogel adhesion: A supramolecular synergy of chemistry, topology, and mechanics. *Adv. Funct. Mater.* **30**, 1901693 (2019).
35. J. Yang *et al*., Design molecular topology for wet–dry adhesion. *ACS Appl. Mater. Interfaces* **11**, 24802–24811 (2019).
36. J. Y. Sun *et al*., Highly stretchable and tough hydrogels. *Nature* **489**, 133–136 (2012).
37. G. Bao *et al*., Ionotronic tough adhesives with intrinsic multifunctionality. *ACS Appl. Mater. Interfaces* **13**, 37849–37861 (2021).
38. X. Liu, J. Liu, S. Lin, X. Zhao, Hydrogel machines. *Mater. Today* **36**, 102–124 (2020).
39. J. Yang, J. Steck, R. Bai, Z. Suo, Topological adhesion. II. Stretchable adhesion. *Extr. Mech. Lett.* **40**, 100891 (2020).
40. N. Gjorevski *et al*., Tissue geometry drives deterministic organoid patterning. *Science* **375**, eaaw9021 (2022).
41. S. Lin *et al*., Stretchable hydrogel electronics and devices. *Adv. Mater.* **28**, 4497–4505 (2016).
42. W. Whyte *et al*., Sustained release of targeted cardiac therapy with a replenishable implanted epicardial reservoir. *Nat. Biomed. Eng.* **2**, 416–428 (2018).
43. D. Vera *et al*., Engineering tissue barrier models on hydrogel microfluidic platforms. *ACS Appl. Mater. Interfaces* **13**, 13920–13933 (2021).
44. A. Tudor *et al*., Fabrication of soft, stimulus-responsive structures with sub-micron resolution via two-photon polymerization of poly (ionic liquid)s. *Mater. Today* **21**, 807–816 (2018).
45. M. Carlotti, V. Mattoli, Functional materials for two-photon polymerization in microfabrication. *Small* **15**, 1902687 (2019).
46. J. Pikul *et al*., Stretchable surfaces with programmable 3D texture morphing for synthetic camouflaging skins. *Science* **358**, 210–214 (2017).